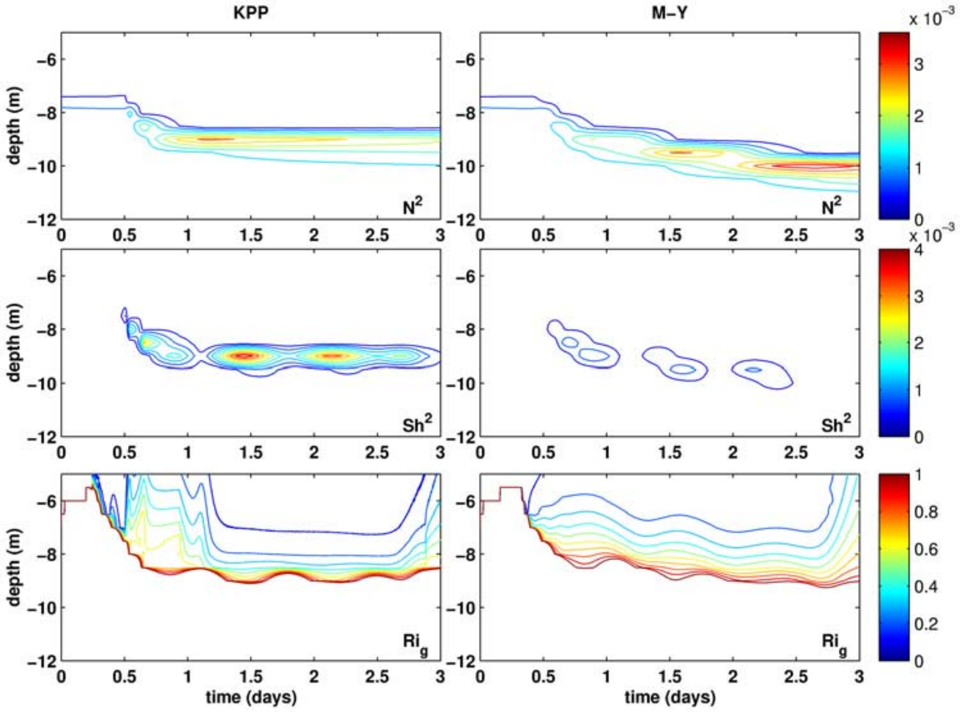

Figure 5. Time-depth contour plots of N^2, velocity shear squared, and gradient Richardson number for the two schemes.

turbulence continues to extend downward for the duration of the wind event with M-Y. Upon cessation of the surface stress, both schemes display a rapid drop off in turbulent mixing.

[48] The time rate of change of potential density in these one-dimensional, horizontally homogenous simulations is equal to the vertical diffusion term,

$$\frac{\partial \rho}{\partial t} = \frac{\partial}{\partial z} K_\rho \frac{\partial \rho}{\partial z} \tag{29}$$

Time versus depth contour plots of this term show how the two schemes deepen the boundary layer and entrain differently (Figure 7). Yellow and red areas in these figures indicate regions where the vertical flux of denser water from the pycnocline is causing the density to rise. Blue regions in these figures occur where the density is locally decreasing because of the deepening of the pycnocline. These are depths which are transitioning from being at the top of the pycnocline to the base of a relatively well mixed boundary layer. As suggested by the earlier figures, the KPP scheme mixes intensely during the first half day of wind forcing but shuts down abruptly at approximately day 1.2. The region of negative flux divergence becomes increasingly thin as the mixing weakens. The Mellor-Yamada parameterization produces periods of enhanced flux of denser water into the boundary layer coinciding with deepening events at approximately an inertial frequency. These events happen concurrently with moderate increases in the mixing coefficient profiles and increases in Sh^2 and N^2 in Figures 5 and 6. While the region of negative flux divergence thins with each pulse in entrainment, unlike KPP, subsequently it broadens.

[49] This suggests that the difference in the response of the two schemes rests in the interplay between the deepening of the boundary layer and the diffusion of the pycnocline upward. The vertical mixing term in the density equation can be separated into two parts.

$$\frac{\partial}{\partial z} K_\rho \frac{\partial \rho}{\partial z} = \frac{\partial K_\rho}{\partial z}\frac{\partial \rho}{\partial z} + K_\rho \frac{\partial^2 \rho}{\partial z^2} \tag{30}$$

At the top of the pycnocline, $\partial_z\rho$ is negative, $\partial_{zz}\rho$ is positive and $\partial_z K\rho$ is positive. Thus the first term on the right-hand side of this equation is negative and associated with the decrease in density due to boundary layer deepening. It acts effectively in the up-gradient direction. The second term acts in the opposite sense and represents the typical ''diffusive'' effect of spreading a scalar from high concentration to low. The KPP simulations are an example of a case in which these mixing terms come to nearly cancel each other at the top of the pycnocline. Figure 8 displays time versus depth contours of $\partial_z\rho$, $\partial_{zz}\rho$ and $\partial_z K_\rho$ for the $N_o/10$ case. The bottom pair of panels shows the two component terms of the vertical mixing. ($\partial_z K_\rho \partial_z \rho$ is contoured in blue. $K_\rho \partial_{zz}\rho$ is contoured in red at the same contouring interval.) Where contours overlie precisely, the two effects cancel, where contours lay ''outside'' of contours of the other color, that effect (deepening of the boundary layer [blue] or spreading of the pycnocline [red]) dominates. Contours are only drawn over a limited range to emphasize the areas where the differences between the schemes occur.

[50] Figure 8 helps explain the sudden change in entrainment rate observed in Figure 3. Strong mixing at the onset of the wind event erodes the stratification while pushing the pycnocline downward. As the boundary layer deepens the